Using Temperature Dependent Fluorescence to Evaluate Singlet Fission Pathways in Tetracene Single Crystals

Chad D. Cruz,[1,3] Eric L. Chronister[2], Christopher J. Bardeen[1,a)]

[1]Department of Chemistry, University of California Riverside, Riverside, CA 92521, USA
[2]Department of Chemistry and Biochemistry, University of Nevada, Las Vegas, 4505 S. Maryland Parkway, Las Vegas NV 89154, USA

Present Address
[3]Nanoscale Device Characterization Division, National Institute of Standards and Technology, 101 Bureau Drive, Gaithersburg, Maryland, 20899, United States

[a)]**Author to whom correspondence should be addressed:** christopher.bardeen@ucr.edu

Abstract

The temperature dependent fluorescence spectrum, decay rate and spin quantum beats are examined in single tetracene crystals to gain insight into the mechanism of singlet fission. Over the temperature range 250 K to 500 K, the vibronic lineshape of the emission indicates that the singlet exciton becomes localized at 400 K. The fission process is insensitive to this localization and exhibits Arrhenius behavior with an activation energy of 550 ± 50 cm^{-1}. The damping rate of the triplet pair spin quantum beats in the delayed fluorescence also exhibits an Arrhenius temperature dependence with an activation energy of 165 ± 70 cm^{-1}. All the data for T>250 K are consistent with direct production of a spatially separated ^{1}(T….T) state via a thermally activated process, analogous to spontaneous parametric downconversion of photons. For temperatures in the range 20 K to 250 K, the singlet exciton continues to undergo a rapid decay on the order of 200 ps, leaving a red-shifted emission that decays on the order of 100 ns. At very long times ($\approx$1 μs) a delayed fluorescence component corresponding to the original S_1 state can still be resolved, unlike in polycrystalline films. A kinetic analysis shows that the redshifted emission seen at lower temperatures cannot be an intermediate in the triplet production. When considered in the context

of other results, our data suggest that the production of triplets in tetracene for temperatures below

250 K is a complex process that is sensitive to the presence of structural defects.

Introduction

Singlet fission (SF) is an excited state relaxation channel in which a spin singlet state (S) converts into a pair of triplet states (TT). Converting one singlet into one triplet (intersystem crossing (ISC)) is spin-forbidden and typically slow, but the ability of a triplet pair to exist in an overall singlet state, usually denoted [1](TT), removes this constraint and allows SF to be very efficient. The study of SF has enjoyed a renaissance over the last 15 years, after its initial discovery and characterization in the 1960s-1980s.[1–4] This renewed interest has been driven mainly by the possibility that it could provide a physical mechanism to surpass the Shockley-Queisser limit on solar energy conversion efficiency.[5–7] But the phenomenon is also of interest because it touches upon many fundamental aspects of exciton dynamics, including delocalization, intermolecular charge and energy transfer, and spin relaxation.

In the study of SF, crystalline tetracene (TET) stands out as a prototypical material that was extensively studied in the early days of the field.[8] The highly efficient endothermic nature of SF in TET makes it an energy efficient SF material, and TET-based chromophores are often used as the active elements in supramolecular assemblies designed to be SF sensitizers.[9–23] Recent demonstrations of the ability of TET to sensitize silicon photovoltaics[24] and function in transistors[25] provide possible paths toward practical applications. The endothermicity also leads to reasonably efficient triplet-triplet fusion or annihilation, which generates a delayed fluorescence (DF) signal that provides a high sensitivity window onto the triplet exciton dynamics.[26] TET crystals also have the fortunate property that the doubly excited spin sublevels of the [1](TT) state can be detected via their quantum beats in the DF signal.[27–31]

Despite years of study, some basic aspects of SF in crystalline TET are still not well understood. These aspects include the role played by singlet state delocalization, the nature of the

^{1}(TT) triplet pair state, and the mechanism by which it decoheres into two independent triplet excitons. Perhaps the most mysterious aspect of SF in TET is its apparent lack of temperature dependence. Given that the triplet and singlet energies $E(T_1)$ and $E(S_1)$ fulfill the inequality $2E(T_1) > E(S_1)$, SF is expected to be an endothermic process with an activation energy ranging from 500 cm^{-1} to 2000 cm^{-1}.[32–35] Although early workers observed a temperature dependent fluorescence yield that they analyzed in terms of this activation energy[36], later work showed that the initial picosecond decay of the S_1 state is remarkably constant over the range 300 K to 4 K.[32,37–39] Interestingly, in the range 300 K to 400 K a clear Arrhenius rate dependence on temperature was found with an activation energy that depended on the sample morphology (polycrystalline thin film versus single crystal).[40] Entropic contributions to the free energy and vibronic coherence have been proposed as possible mechanisms for the anomalous dependence of TET's fission rate on temperature[37,41,42], but there is still no universally accepted explanation.

The difficulty of making a simple self-consistent model for SF in TET raises the possibility that multiple kinetic pathways and intermediates are involved. The standard mechanism for SF postulates a single pathway that follows the sequence $S_1 \xrightarrow{i)} {}^1(TT) \xrightarrow{ii)} {}^1(T....T) \xrightarrow{iii)} T + T$ as shown schematically in Figure 1a. Note that steps *ii)* and *iii)* do not have to occur simultaneously, since Scholes showed theoretically that the triplet motion can proceed without loss of spin coherence.[43] Recently, Xiao et al. performed a detailed study that analyzed the frequency and structure of the beats and concluded that the exchange interaction between the triplet excitons that comprise the ^{1}(TT) state was too small to be detected.[31] This result was consistent with the analysis of previous workers[29], leading to the conclusion that the triplet pairs created by SF are spatially separated and effectively noninteracting. They postulated a two-channel process for SF in TET where the standard process in Figure 1a is accompanied by a second pathway in which the separated pair is

formed directly by SF, $S_1 \rightarrow {}^1(T....T)$, as shown in Figure 1b. The physical origin of the two pathways was left unexplored, as was how this mechanism might explain the anomalous temperature dependence of SF in TET. The possibility of alternate pathways for triplet production has also been suggested by recent low-temperature ESR studies by Bayliss et al.[44] and transient absorption studies by Wan et al.[45], both of which suggest that ISC can generate a large fraction of triplets at low temperatures, possibly via trapping to defects. Two defect mediated pathways for SF and ISC are shown in Figures 1c and 1d. Most workers have assumed that ISC in crystalline TET is negligible, despite its yield of 0.62 in solution.[46] Anthracene has a similar ISC quantum yield in solution, but exhibits a high fluorescence quantum yield in crystal form, presumably due to singlet energy shifts in the crystal[47] combined with a rigid environment that suppresses energy fluctuations that facilitate ISC in solution.[48] TET is similar to anthracene in terms of its molecular photophysics, so enhanced ISC in the crystal would likely result from a higher density of defects that enable ISC.

In this paper, we try to clarify the situation by using time-resolved fluorescence spectroscopy to look at the dynamics of the triplet pair state in single crystal TET. The goal is to determine which of the kinetic pathways in Figure 1 are consistent with the data. We are particularly interested in whether the direct route to the ${}^1(T....T)$ state (Figure 1b) plays a large role in TET, and whether this process can also help explain the anomalous dependence of SF on temperature. Disparate results on single crystals, along with earlier studies on polycrystalline films, are compared in order to gain insight into the potential role of defects. Ultimately, we are interested in determining whether the SF process in high quality TET crystals is analogous to spontaneous parametric downconversion (SPDC) of photons in nonlinear optical crystals.[49] If SF directly produces a pair of noninteracting, spatially separated triplet excitons that can maintain

spin entanglement, we think this could provide an interesting system for testing the basic properties of entangled state quantum mechanics.[50]

Experimental

Tetracene purchased from Sigma-Aldrich (benz[b]anthracene, sublimed grade 99.99%) was used as received. To make single crystals, ~ 7 mg of tetracene is dissolved in 50 mL of toluene and sonicated for $\sim$20 min in the dark. Under only red ambient lighting, the solution is filtered through a Whatman Qualitative #1 filter into a separate precleaned flask which is covered in aluminum foil to prevent inadvertent light exposure. Glass slides are cleaned by bathing in concentrated hydrochloric acid for at least 4 h. The slides are rinsed with deionized water followed by methanol and then allowed to dry. The filtered tetracene solution is then drop cast onto the cleaned glass or silanized glass slides and allowed to evaporate in a dark drawer for a minimum of 1 h. Using an optical microscope, crystals which resemble a stretched hexagon are identified for further measurements. For low temperature studies (20 K to 250 K), the crystals are left uncovered and mounted on the heat exchanger of a Janis Research vacuum cryostat (10^{-3} Pa) fitted with optical windows. Indium metal is placed between the glass slide and cryostat heat exchanger to obtain good thermal contact. For high temperature measurements (294 K to 495 K), the crystals require protection to prevent sublimation at T > 350 K. In a glove bag filled with nitrogen, a drop of fomblin oil (PFPE) is placed over the crystal followed by a glass coverslip. To seal the sample, copper room temperature vulcanizing (RTV) sealant (Permatex 81878 Ultra Copper Maximum Temperature Silicone Sealant, rated to 644 K) is placed at the edges of the coverslip to adhere it to the glass slide. After a 24 h curing period, the samples are impervious to sublimation at elevated temperature.

Time-resolved fluorescence measurements are performed with an 80 MHz Coherent Vitesse Ti:Sapphire oscillator. For all measurements, the repetition rate of the Vitesse laser is lowered to 100 kHz using a Pockels cell controlled with a ConOptics pulse picking system. The 800 nm fundamental beam is frequency doubled using a BBO crystal to generate the 400 nm excitation beam. The fluence is varied with a set of neutral density filters and calculated by measuring the power immediately before the sample with a power meter. The Gaussian beam waist is determined to be 33 µm (FWHM) with a knife edge measurement. The laser fluence remained between 1 µJ/cm^2 and 5 µJ/cm^2 to avoid the exciton-exciton annihilation that complicates the photodynamics at fluences above 6 µJ/cm^2.[32] No variations in the fluorescence decay at short or long times are observed over the range of fluences used in this work. A Hamamatsu C4334 Streakscope is used to collect the time-resolved fluorescence spectra. The streak camera provides both spectral and dynamical data from the sample with 2.5 nm and 20 ps spectral and temporal resolution, respectively. A 450 nm long pass filter is placed before the streak camera to minimize the contribution of laser scatter to the signal.

Results and Discussion

Single TET crystals are grown by solvent evaporation on a glass slide as in our previous work.[29,40] This method has the advantage of consistently being able to grow large area ($\approx$ 1 mm^2) ultrathin ($\approx$0.1 mm) crystals (Supporting Information) that are easy to find and allow us to neglect self-absorption effects in the fluorescence spectra. In order to measure the singlet decay over a wider temperature range, we submerged the TET crystal in an inert fluoropolymer oil and glued a second glass coverslip on top of it with high-temperature epoxy. Without the oil, we found that the crystals sublimed inside the sealed glass chamber and recrystallized near the edges. The

combination of oil and epoxy sealing allowed us to raise the crystal temperature to 495 K, still well below TET's melting point of 630 K. As the temperature increased, the spectrum of the prompt fluorescence (integrated over the 0 ns to 1 ns window) changed in a systematic way, with the 0-0 vibronic peak losing intensity relative to the 0-1 peak (Figure 2a). These data extend the results from our group and others that previously studied the temperature range 300 K to 4 K. At ≈450 K, we started to observe the signature peak of monomeric TET at 490 nm, indicating that some of the crystal was dissolving in the surrounding oil. When the crystal emission line-shape was fit to a series of Gaussians, the relative 0-0/0-1 peak ratios could be extracted and then plotted as a function of temperature. This plot, shown in Figure 2b, is linear over the range 300 K to 400 K, as predicted by the theory of Spano that describes Frenkel exciton delocalization.[51] At 400 K, the 0-0/0-1 ratio becomes similar to that of monomeric TET in solution and then remains constant up to 500 K. We interpret this as the point at which the exciton coherence length becomes comparable to a single molecule, i.e. it is localized on a single TET site. Thus dynamics measured over the range 400-500 K likely proceed in the absence of singlet delocalization.

Figure 3a shows the decay of the prompt fluorescence integrated from 510 nm to 650 nm in the 1 ns time window. The fluorescence decay time, as determined by fitting the first natural log of the decay, changes from 250 ps to 100 ps over the range 250 K to 495 K. This variation is well-reproduced by an Arrhenius process with an effective singlet decay rate k_{S1}, which we assume reflects the fission rate and is given by

$$k_{S1} = A_1 \exp[-E_{a1}/k_B T] \tag{1}$$

A plot of $\log(k_{S1})$ versus $1/T$ is linear and yields a prefactor $A_1 = 10^8$ s^{-1} and $E_{a1} = 550 \pm 50$ cm^{-1} (Figure 3b) , where the uncertainty is given by the standard deviation of the slope fit to the data using a linear regression, in good agreement with previous results that only went up to 400 K.[40]

The smooth Arrhenius behavior over the entire range suggests that S_1 exciton localization at 400 K has little or no impact on the SF rate.

Finally, while the prompt fluorescence decay showed a strong temperature dependence, the DF was found to be relatively insensitive over the same range (Figure 4a). This insensitivity extended to the spin quantum beats (QBs), as shown in Figure 4b. After subtracting the background to isolate the oscillatory signal, we found that an obvious beat signal persisted up to 495 K, when the crystal was starting to dissolve. The oscillations could be fit using a damped cosine function,

$$y(t) = A \cos(2\pi\nu t - \phi)\, e^{-\alpha t} \qquad (2)$$

where A is the amplitude of the oscillations, t is the time, ν is the frequency, ϕ is the phase and α is the damping coefficient. The frequency ν is set to 1.08 GHz per previous results on quantum beats in crystalline tetracene.[29,52] The rest of the parameters are allowed to vary. This procedure is a somewhat crude approximation of the oscillations since multiple beat frequencies are present in the oscillations and their contributions may change with temperature. Fitting the data using Equation (2) allows us to extract α for each temperature. A plot of $\log(\alpha)$ versus 1/T is shown in Figure 5 and yields a linear Arrhenius plot with a slope that gives an activation energy E_{a2} of 160 ± 70 cm^{-1}, where the uncertainty is given by the standard deviation of the slope fit to the data with a weighted linear regression. The low activation energy for α is consistent with the lack of dramatic changes in the oscillations in Figure 4b. The fact that additional high frequency QBs become more pronounced at higher temperatures, consistent with more impulsive excitation due to more rapid SF, probably contributes to the error in E_{a2}.

The damping rate α can arise from pure spin dephasing of the bound pair state, or from physical separation of the triplets that decreases the probability of geminate recombination. If we

assume that the disappearance of the oscillations is the result of triplet pair dissociation, i.e. ^{1}(TT) $\rightarrow$ ^{1}(T....T), then E_{a2} would reflect the triplet pair binding energy. In fact, $E_{a2} = 160$ cm^{-1} is comparable to the value of ~250 cm^{-1} estimated by Sirringhaus and coworkers for the binding energy of the ^{1}(TT) state in a variety of SF materials.[53] But the lifetime of the bound ^{1}(TT) pair has been estimated to be less than 100 ps in crystalline tetracene[45], much less than our measured damping time $(1/\alpha)$ of 3 ns at room temperature. Furthermore, previous analyses showed that the oscillations could be well-described using only the D* and E* zero-field parameters for noninteracting triplet excitons.[29,31] Magnetic interactions between closely bound triplets tend to lead to energy shifts and the appearance of mixed spin states, as demonstrated in multiple electron spin resonance experiments on bound triplet pairs.[54-59] The absence of such shifts in the QB frequencies leads us to suspect that α's temperature dependence reflects an increased triplet diffusion rate that makes geminate recombination of the ^{1}(T....T) state less probable at higher temperatures. This activation energy is comparable to that deduced for triplet exciton diffusion in molecular crystals like dibromobenzene and anthracene.[60,61] Note that the long-time (>20 ns) DF signal is even less sensitive to temperature, since even if the triplet excitons do not recombine as spin-coherent pairs, they can still recombine as free triplets (both geminate and nongeminate) and contribute to the DF signal.

Over the temperature range 250 K to 500 K, single crystal TET appears to be dominated by the direct process $S_1 \rightarrow$ ^{1}(T....T) that follows standard Arrhenius behavior and is not affected by the amount of S_1 delocalization. But when the temperature drops below 200 K, the time-resolved fluorescence behavior undergoes a distinct change. First, the QBs can no longer be discerned in the DF signal. This is not entirely surprising. Extrapolation of the Arrhenius curve in Figure 3b predicts that $1/k_{S1}$ will become 1.1 ns at 200 K, and in this limit SF will be too slow to impulsively

excite the spin QBs. But this is not the only change in the fluorescence behavior. For the early time decay, we still see the pronounced enhancement of the 0-0 peak over the 0-1 peak, indicative of increased coherence length of the exciton at lower temperatures, as observed previously (Supporting Information).[62–64] Furthermore, there is a rapid ≈250 ps decay of this signal all the way down to 20 K, again consistent with previous observations (Figure 6a). This persistent fast decay of the singlet state, also observed in polycrystalline films, has been taken as evidence for the temperature independence of SF in this crystal.

More dramatic are the changes in the fluorescence decay on the longer timescale of 20 ns to 100 ns. At room temperature and higher, the DF spectrum is identical to the initial S_1 emission and does not change over the course of the fluorescence decay that spans microseconds. This is what is expected for traditional DF that arises after SF forms free triplets whose fusion regenerates the original S_1 state. The microsecond DF signal above 250 K is replaced by a new emitting species with a nanosecond lifetime that lengthens at lower temperatures (Figure 6b). In Figure 7, we show a set of fluorescence spectra acquired in different time windows. At all temperatures, the initial spectrum (0 ns to 1 ns) reflects the delocalized S_1 exciton as observed previously. At 250 K, there is a slight redshift over 1 μs, but the spectral shape remains constant with a dominant 0-0 peak at ≈530 nm. At 150 K and 77 K, on the other hand, the spectra in the 1 ns to 40 ns time windows are dominated by structured peaks in the 550 nm to 600 nm region. Interestingly, at even longer times, the 0-0 peak becomes dominant again and the original S_1 spectrum is recovered. At 20 K, the 570 nm feature is even better resolved and persists into the microsecond time window, so we no longer recover the full S_1 spectrum observed in the 0-1 ns window. The long-term survival of the 0-0 peak, which was not observed in our previous low-temperature studies of TET

polycrystalline films, is especially pronounced at the intermediate temperatures of 150 K and 77 K.

If SF is assumed to proceed sequentially through the ^{1}(TT) state and on to the ^{1}(T….T) state (Figure 1a), then it is natural to assign the red emission to the ^{1}(TT) bound state that rapidly dissociates at high temperatures but becomes trapped at lower temperatures. But if the ^{1}(TT) bound state is a required intermediate on the way to ^{1}(T….T), this places some constraints on the evolution of the fluorescence spectrum. Kinetic modeling can be used to determine whether the sequential mechanism in Figure 1a is consistent with the observed spectral behavior.

Consider the general 3-state kinetic scheme outlined in Figure 8. This scheme leads to three coupled differential equations:

$$\frac{dN_1}{dt} = -(k_{12} + k_{13})N_1 + k_{21}N_2 + k_{31}N_3 - k_1N_1 \tag{3a}$$

$$\frac{dN_2}{dt} = -(k_{21} + k_{23})N_2 + k_{12}N_1 + k_{32}N_3 - k_2N_2 \tag{3b}$$

$$\frac{dN_3}{dt} = -(k_{32} + k_{31})N_3 + k_{13}N_1 + k_{23}N_2 - k_3N_3 \tag{3c}$$

where state 1 represents S_1, state 2 represents the ^{1}(TT) and state 3 represents the ^{1}(T….T) and free triplet T + T populations. We assume that states 1 and 2 can be monitored by their emission, while state 3 (corresponding to separated triplets) is dark. We are interested in the ratio N_1/N_2, which determines the ratio of high versus low energy emission signals. At very early times, only N_1 exists. As the population continues to relax, a temporary equilibrium will be established between states 1 and 2, with $N_1/N_2 = k_{21}/k_{12}$. At longer times, an equilibrium will be established between all three levels with N_3 acting as a long-lived reservoir of population ($k_3 \sim 0$). Now we assume that N_1 and N_2 establish a quasi-equilibrium such that $dN1/dt = dN2/dt = 0$, leading to the general result:

$$\left(\frac{N_1}{N_2}\right)_{eq} = \frac{\dfrac{k_{31}}{\gamma_1} + \dfrac{k_{21}}{\gamma_1}\dfrac{\gamma_1\gamma_2}{(\gamma_1\gamma_2 - k_{12}k_{21})}\left(\dfrac{k_{32}}{\gamma_2} + \dfrac{k_{12}k_{31}}{\gamma_1\gamma_2}\right)}{\dfrac{\gamma_1\gamma_2}{(\gamma_1\gamma_2 - k_{12}k_{21})}\left(\dfrac{k_{32}}{\gamma_2} + \dfrac{k_{12}k_{31}}{\gamma_1\gamma_2}\right)} \qquad (2)$$

$$\gamma_1 = k_{12} + k_{13} + k_1$$
$$\gamma_2 = k_{21} + k_{23} + k_2$$

We now consider two limiting cases corresponding to different mechanisms in Figure 1:

A) Sequential path (Figure 1a) , for which $k_{13}=k_{31}=0$, which leads to

$$\left(\frac{N_1}{N_2}\right)_{eq} = \frac{k_{21}}{k_{12} + k_1} \qquad (4)$$

In other words, the final N_1/N_2 ratio must be equal to or less than the early time N_1/N_2 ratio – there cannot be a situation in which the N_1 emission dominates in both very early and very late time windows.

B) Parallel paths for the S_1 state (Figures 1a and 1b), with $k_{23}=k_{32}=0$, which leads to

$$\left(\frac{N_1}{N_2}\right)_{eq} = \frac{k_{21} + k_2}{k_{12}} \qquad (5)$$

From this expression, we see that the long-time ratio can be larger than the initial ratio simply by allowing a large k_2 value, which makes N_2 decay quickly while N_3 replenishes N_1.

C) Irreversible defect trapping and triplet state pathways ($k_{21}=k_{23}=k_{32}=0$), which leads to

$$\left(\frac{N_1}{N_2}\right)_{eq} = \frac{k_2}{k_{12}} \qquad (5)$$

Again, the ability to replenish state 1 from state 3, while state 2 decays rapidly, allows for an apparent revival of the state 1 emission at long times.

These expressions based on quasi-equilibrium calculations are confirmed by numerically solving the kinetic equations as shown in the Supporting Information. The time-dependent calculations confirm that the sequential model A) leads to a decreasing N_1/N_2 ratio at all times, while scenarios B) and C) can give rise to a N_1/N_2 ratio that first decreases but then increases before reaching a steady state. Such behavior qualitatively resembles the decrease in red emission (state 2) relative to the higher energy S_1 emission (state 1) seen experimentally.

Interestingly, when the populations all originate from a common S_1 state, we were unable to generate a case where the N_1 population dominated the long-time emission – rapid relaxation into state 2 always maintained $N_1/N_2<1$. In order to explain the large amplitude of S_1 emission at long times, we would have to have two separate populations where one of them does not relax to the red-emitting state at all. So an alternative scenario to A)-C) above is one in which two distinct S_1 subpopulations exist, one of which bypasses relaxation to the red-emitting state to directly create long-lived triplets.

The analysis in the previous two paragraphs shows that if we assume the S_1 emission at very long times is due to DF from triplet-triplet fusion, then the pathway that produces these triplets must be independent of that which produces the red emitting species. The precise nature of the redshifted emission remains an open question. One possibility is that it is associated with a "stalled" ^{1}(TT) state that cannot complete the fission process. If this is the case, there must be another source of triplets at low temperature to produce the DF. Alternatively, it could be associated with structural defects. These defects could be created during crystal growth at room temperature or induced as the temperature decreases and the crystal undergoes phase changes that create new grain boundaries.[65–68] In either case, we again have the requirement that triplet fusion back to the S_1 state must be able to bypass these defects to avoid regenerating the red emission.

We note that the crystals did not show any difference in behavior when warmed back up to room temperature, suggesting that any defect creation due to phase changes was reversible. One thing we do know is that the direct SF pathway identified in the range 300-500 K will not be competitive at these lower temperatures, since it is calculated to decline to 1.1×10^9 s^{-1} at 200 K, 3.0×10^8 s^{-1} at 150 K, and 2.0×10^6 s^{-1} at 77 K. It is possible that an alternative path for SF exists at low temperatures, for example tunneling, but again this pathway would proceed independently of the red-emitting species. The most important conclusion we can draw is that the red emission does not correspond to the ^{1}(TT) intermediate in Figure 1a. We emphasize that this conclusion rests on our ability to observe long-lived DF signal from the original S_1 state in the single crystals, which was absent in our polycrystalline films.[32]

If we assume that triplets must be produced at T<200K and are byproducts of the defect mediated trapping followed by SF and/or ISC, we must assume that our TET crystals have a relatively high density of defects. This is actually consistent with other observations. Unlike anthracene, TET cannot be zone-refined and always contains appreciable concentrations of chemical impurities[69] which can lead to packing defects in the crystal. While high-purity anthracene crystals give rise to low temperature (4 K) photoluminescence peaks with widths on the order of 10 cm^{-1} [70,71], structural defects can broaden lines in this crystal.[72,73] In contrast, crystalline TET consistently gives rise to 4 K photoluminescence peaks with widths on the order of 300 cm^{-1}, possibly indicative of a high density of defects. If TET is prone to defective growth, it would also help explain some of the spread in kinetic measurements reported in the literature. For example, there are large differences in the initial SF rates obtained by performing the same room temperature visible/near-infrared transient absorption experiment on single crystals, which have been reported to range from 25ps to 156 ps.[45,74–78] Single crystals should provide the most

reproducible samples because they presumably avoid polymorphism associated with the growth of polycrystalline films on surfaces[79], which is presumably responsible for the large range of SF times (22 ps to 125 ps) reported for this class of samples.[32,39,80] Assuming that experimental artifacts like nonlinear exciton annihilation dynamics have been correctly accounted for, then we can conclude that this variation results from variable crystal quality.

The singlet exciton diffusion rate is estimated to range from (10^{-3} to 10^{-2}) cm^2/s[81–83], which would allow it to cover roughly 10 nm within 100 ps. In a trap-dominated scenario, the intrinsic SF process competes with singlet diffusion to defect sites, whose density varies from sample to sample. The approximately constant S_1 decay from 250 K to 4 K would then indicate that the singlet diffusion rate is temperature independent over this range. Trapping to some distribution of emissive defects would be followed by either relaxation back to S_0, or the generation of long-lived triplets via slow SF or ISC. It is also possible that there exist local regions within a single crystal that are largely defect-free and the data represents a spatial average over different domains. Measurements with high spatial resolution might help distinguish between these possibilities.

We note that our analysis rests on the assumption that the fluorescence signal is an accurate reporter of the overall singlet population. The strength of the fluorescence experiment is that its high sensitivity allows experiments to be carried out at low excitation fluences, avoiding the singlet-singlet annihilation dynamics and heating artifacts that can affect transient absorption experiments. Furthermore, the delayed fluorescence QBs provide an unambiguous detection of the ^{1}(T….T) state. But the fluorescence experiment is only sensitive to emissive species. If there exists a parallel channel for SF via a dark singlet state that generates triplets but does not give rise to significant fluorescence, then transient absorption becomes the more reliable method to probe such sates. So a possible objection to our interpretation is that the fluorescence experiments are

simply missing the bulk of the S_1 decay into dark states that have different kinetics. The fact that fluorescence lifetime experiments consistently yield a longer singlet lifetime (on the order of 200 ps to 250 ps)[31,33,40,84–88] than transient absorption experiments suggests that there could be a systematic discrepancy between the two types of experiments. We previously showed that the decay of the triplet absorption signal at 800 nm and the delayed fluorescence paralleled each other on the 100 ns timescale for polycrystalline films[89], but we have not done a similar consistency check for single crystals. To our knowledge, there has not been a combined fluorescence-transient absorption study of single TET crystals to determine if one kinetic model can provide a self-consistent description of both experiments at all excitation densities.

Conclusion

One goal of this paper has been to present new results on the temperature dependence of the S_1 decay rate and spin quantum beats in TET single crystals. All the fluorescence data for T>200 K are consistent with direct production of the spatially separated $^1(T….T)$ state via a thermally activated process that is insensitive to the delocalization of the parent S_1 exciton. The second goal of the paper was to examine whether the $^1(TT)$ intermediate might be observed at temperatures below 300 K. We conclude that the redshifted emission seen at lower temperatures cannot be a kinetic intermediate on the way to the $^1(T….T)$ state but may instead reflect a trapped singlet state. The observation of delayed fluorescence even at low (20 K) temperatures shows that triplets are still being produced, but the mechanism is not the same thermally activated process that operates at high temperatures. While this hypothesis can explain most of the experimental observations on TET, conclusive proof probably requires performing multiple measurements (transient absorption, fluorescence, electron spin resonance) on the same crystal sample while

17

characterizing the crystallinity using X-ray or electron diffraction and impurity content, possibly by mass spectrometry. This is a daunting project, but it might prove that SF in TET is simpler than it previously appeared.

The fluorescence data suggest that high temperature SF in crystalline TET may be analogous to spontaneous parametric downconversion of photons, where a single particle splits into a pair of unbound, non-interacting particles whose behavior is correlated by their spin entanglement generated at the moment of creation. It appears that typical TET crystals may have a high defect density that obscures this process, especially at low temperatures. However, it may be possible to engineer SF molecular crystals where direct production of the $^1(T....T)$ state is dominant at all temperatures. Given the long lifetimes and high diffusion rates of triplet excitons in high quality polyacene crystals, it is possible to envision utilizing such spatially separated, spin-entangled triplet pairs for experiments analogous to those done with photon pairs generated by SPDC.[50]

Supplementary Material

See Supplementary Material for crystal images, low temperature PL and kinetic rates used in the model.

Acknowledgments

or endorsement by the National Institute of Standards and Technology, nor is it intended to imply

that the materials or equipment identified are necessarily the best available for the purpose.

<u>Data Availability</u>

The data that support the findings of this study are available from the corresponding author

upon reasonable request.

References

(1)   Swenberg, C. E.; Geacintov, N. E. Exciton Interactions in Organic Solids. In *Organic Molecular Photophysics*; Birks, J. B., Ed.; J. Wiley & Sons: London, 1973; Vol. 1, pp 489–564.

(2)   Pope, M.; Swenberg, C. E. *Electronic Processes in Organic Crystals and Polymers*; Oxford University Press: New York, 1999.

(3)   Smith, M. B.; Michl, J. Recent Advances in Singlet Fission. *Ann. Rev. Phys. Chem.* **2013**, *64*, 361–386.

(4)   Smith, M. B.; Michl, J. Singlet Fission. *Chem. Rev.* **2010**, *110*, 6891–6936.

(5)   Hanna, M. C.; Nozik, A. J. Solar Conversion Efficiency of Photovoltaic and Photoelectrolysis Cells with Carrier Multiplication Absorbers. *J. Appl. Phys.* **2006**, *100*, 074510/1-074510/8.

(6)   Shpaisman, H.; Nitsoo, O.; Lubomirsky, I.; Cahen, D. Can Up- and down-Conversion and Multi-Exciton Generation Improve Photovoltaics. *Sol. Ener. Mater. Sol. Cells* **2008**, *92*, 1541–1546.

(7)   Trupke, T.; Green, M. A.; Wurfel, P. Improving Solar Cell Efficiencies by Down-Conversion of High-Energy Photons. *J. Appl. Phys.* **2002**, *92*, 1668–1674.

(8)   Pope, M.; Geacintov, N. E. F. V. Singlet Exciton Fission and Triplet-Triplet Exciton Fusion in Crystalline Tetracene. *Molec. Cryst.* **1969**, *6*, 83–104.

(9)   Gilligan, A. T.; Miller, E. G.; Sammakia, T.; Damrauer, N. H. Using Structurally Well-Defined Norbornyl-Bridged Acene Dimers to Map a Mechanistic Landscape for Correlated Triplet Formation in Singlet Fission. *J. Am. Chem. Soc.* **2019**, *141*, 5961−5971.

(10)   Korovina, N. V.; Joy, J.; Feng, X.; Feltenberger, C.; Krylov, A. I.; Bradforth, S. E.; Thompson, M. E. Linker-Dependent Singlet Fission in Tetracene Dimers. *J. Am. Chem. Soc.* **2018**, *140*, 10179−10190.

(11)   Mora-Fuentes, J. P.; Papadopoulos, I.; Thiel, D.; Lvarez-Boto, R.; Cortizo-Lacalle, D.; Clark, T.; Melle-Franco, M.; Guldi, D. M.; Mateo-Alonso, A. Singlet Fission in Pyrene-Fused Azaacene Dimers. *Angew. Chem. Int. Ed.* **2020**, *59*, 1113 –1117.

(12)   Pun, A. B.; Asadpoordarvish, A.; Tayebjee, M. J. Y.; Kumarasamy, E.; Niesner, D.; McCamey, D. R.; Sanders, S. N.; Campos, L. M.; Sfeir, M. Y. Ultra-Fast Intramolecular Singlet Fission to Persistent Multiexcitons by Molecular Design. *Nat. Chem.* **2019**, *11*, 821–827.

(13)   Muller, A. M.; Avlasevich, Y. S.; Mullen, K.; Bardeen, C. J. Evidence for Exciton Fission and Fusion in a Covalently Linked Tetracene Dimer. *Chem. Phys. Lett.* **2006**, *421*, 518–522.

(14)   Muller, A. M.; Avlasevich, Y. S.; Schoeller, W. W.; Mullen, K.; Bardeen, C. J. Exciton Fission and Fusion in Bis(Tetracene) Molecules with Different Covalent Linker Structures. *J. Am. Chem. Soc.* **2007**, *129*, 14240–14250.

(15)   Liu, H.; Nichols, V. M.; Shen, L.; Jahansouz, S.; Chen, Y.; Hanson, K. M.; Bardeen, C. J.; Li, X. Synthesis and Photophysical Properties of a "Face-to-Face" Stacked Tetracene Dimer. *Phys. Chem. Chem. Phys.* **2015**, *17*, 6523–6531.

(16)   Nakamura, S.; Sakai, H.; Nagashima, H.; Kobori, Y.; Tkachenko, N. V.; Hasobe, T. Quantitative Sequential Photoenergy Conversion Process from Singlet Fission to Intermolecular Two-Electron Transfers Utilizing Tetracene Dimer. *ACS Energy Lett.* **2019**, *4*, 26−31.

(17)   Wang, X.; Wang, R.; Shen, L.; Tang, Z.; Wen, C.; Dong, B.; Liu, H.; Zhang, C.; Li, X.

Intramolecular Singlet Fission in a Face-to-Face Stacked Tetracene Trimer. *Phys. Chem. Chem. Phys.* **2018**, *20*, 6330–6336.

(18)   Cook, J. D.; Carey, T. J.; Arias, D. H.; Johnson, J. C.; Damrauer, N. H. Solvent-Controlled Branching of Localized versus Delocalized Singlet Exciton States and Equilibration with Charge Transfer in a Structurally Well-Defined Tetracene Dimer. *J. Phys. Chem. A* **2017**, *121*, 9229−9242.

(19)   Cook, J. D.; Carey, T. J.; Damrauer, N. H. Solution-Phase Singlet Fission in a Structurally Well-Defined Norbornyl-Bridged Tetracene Dimer. *J. Phys. Chem. A* **2016**, *120*, 4473−4481.

(20)   Korovina, N. V.; Das, S.; Nett, Z.; Feng, X.; Joy, J.; Haiges, R.; Krylov, A. I.; Bradforth, S. E.; Thompson, M. E. Singlet Fission in a Covalently Linked Cofacial Alkynyltetracene Dimer. *J. Am. Chem. Soc.* **2016**, *138*, 617−627.

(21)   Alvertis, A. M.; Lukman, S.; Hele, T. J. H.; Fuemmeler, E. G.; Feng, J.; Wu, J.; Greenham, N. C.; Chin, A. W.; Musser, A. J. Switching between Coherent and Incoherent Singlet Fission via Solvent-Induced Symmetry Breaking. *J. Am. Chem. Soc.* **2019**, *141*, 17558−17570.

(22)   Yamakado, T.; Takahashi, S.; Watanabe, K.; Matsumoto, Y.; Osuka, A.; Saito, S. Conformational Planarization versus Singlet Fission: Distinct Excited- State Dynamics of Cyclooctatetraene-Fused Acene Dimers. *Angew. Chem. Int. Ed.* **2018**, *57*, 5438 –5443.

(23)   Pun, A. B.; Sanders, S. N.; Kumarasamy, E.; Sfeir, M. Y.; Congreve, D. N.; Campos, L. M. Triplet Harvesting from Intramolecular Singlet Fission in Polytetracene. *Adv. Mater.* **2017**, *29*, 1701416.

(24)   Einzinger, M.; Wu, T.; Kompalla, J. F.; Smith, H. L.; Perkinson, C. F.; Nienhaus, L.; Wieghold, S.; Congreve, D. N.; Kahn, A.; Bawendi, M. G.; Baldo, M. A. Sensitization of Silicon by Singlet Exciton Fission in Tetracene. *Nature* **2019**, *571*, 90–94.

(25)   Jang, H.-J.; Bittle, E. G.; Zhang, Q.; Biacchi, A. J.; Richter, C. A.; Gundlach, D. J. Electrical Detection of Singlet Fission in Single Crystal Tetracene Transistors. **2019**, *13*, 616−623.

(26)   Burdett, J. J.; Bardeen, C. J. The Dynamics of Singlet Fission in Crystalline Tetracene and Covalent Analogs. *Acc. Chem. Res.* **2013**, *46*, 1312–1320.

(27)   Chabr, M.; Wild, U. P.; Funfschilling, J.; Zschokke-Granacher, I. Quantum Beats of Prompt Fluorescence in Tetracene Crystals. *Chem. Phys.* **1981**, *57*, 425–430.

(28)   Funfschilling, J.; Zschokke-Granacher, I.; Canonica, S.; Wild, U. P. Quantum Beats in the Fluorescence Decay of Tetracene Crystals. *Helv. Phys. Acta* **1985**, *58*, 347–354.

(29)   Burdett, J. J.; Bardeen, C. J. Quantum Beats in Crystalline Tetracene Delayed Fluorescence Due to Triplet Pair Coherences Produced by Direct Singlet Fission. *J. Am. Chem. Soc.* **2012**, *134*, 8597–8607.

(30)   Wang, R.; Zhang, C.; Zhang, B.; Liu, Y.; Wang, X.; Xiao, M. Magnetic Dipolar Interaction between Correlated Triplets Created by Singlet Fission in Tetracene Crystals. *Nat. Commun.* **2015**, *6*, 8602.

(31)   Wang, Z.; Zhang, C.; Wang, R.; Wang, G.; Wang, X.; Xiao, M. Weakly Coupled Triplet Pair States Probed by Quantum Beating in Delayed Fluorescence in Tetracene Crystals. *J. Chem. Phys.* **2019**, *151*, 134309.

(32)   Burdett, J. J.; Gosztola, D.; Bardeen, C. J. The Dependence of Singlet Exciton Relaxation on Excitation Density and Temperature in Polycrystalline Tetracene Thin Films: Kinetic Evidence for a Dark Intermediate State and Implications for Singlet Fission. *J. Chem.*

Phys. **2011**, *135*, 214508.

(33)   Arnold, S.; Whitten, W. B. Temperature Dependence of the Triplet Exciton Yield in Fission and Fusion in Tetracene. *J. Chem. Phys.* **1981**, *75*, 1166–1169.

(34)   Groff, R. P.; Avakian, P.; Merrifield, R. E. Coexistence of Exciton Fission and Fusion in Tetracene Crystals. *Phys. Rev. B* **1970**, *1*, 815–817.

(35)   Tomkiewicz, Y.; Groff, R. P.; Avakian, P. Spectroscopic Approach to Energetics of Exciton Fission and Fusion in Tetracene Crystals. *J. Chem. Phys.* **1971**, *54*, 4504–4507.

(36)   Geacintov, N.; Pope, M.; Vogel, F. Effect of Magnetic Field on the Fluorescence of Tetracene Crystals: Exciton Fission. *Phys. Rev. Lett.* **1969**, *22*, 593–596.

(37)   Chan, W. L.; Ligges, M.; Zhu, X. Y. The Energy Barrier in Singlet Fission Can Be Overcome through Coherent Coupling and Entropic Gain. *Nat. Chem.* **2012**, *4*, 840–845.

(38)   Tayebjee, M. J. Y.; Clady, R. G. C. R.; Schmidt, T. W. The Exciton Dynamics in Tetracene Thin Films. *PhysChemChemPhys* **2013**, *15*, 14797–14805.

(39)   Wilson, M. W. B.; Rao, A.; Johnson, K.; Gelinas, S.; Pietro, R. di; Clark, J.; Friend, R. H. Temperature-Independent Singlet Exciton Fission in Tetracene. *J. Am. Chem. Soc.* **2013**, *135*, 16680–16688.

(40)   Piland, G. B.; Bardeen, C. J. How Morphology Affects Singlet Fission in Crystalline Tetracene. *J. Phys. Chem. Lett.* **2015**, *6*, 1841–1846.

(41)   Kolomeisky, A. B.; Feng, X.; Krylov, A. I. A Simple Kinetic Model for Singlet Fission: A Role of Electronic and Entropic Contributions to Macroscopic Rates. *J. Phys. Chem. C* **2014**, *118*, 5188−5195.

(42)   Morrison, A. F.; Herbert, J. M. Evidence for Singlet Fission Driven by Vibronic Coherence in Crystalline Tetracene. *J. Phys. Chem. Lett.* **2017**, *8*, 1442−1448.

(43)   Scholes, G. D. Correlated Pair States Formed by Singlet Fission and Exciton−Exciton Annihilation. *J. Phys. Chem. A* **2015**, *119*, 12699−12705.

(44)   Bayliss, S. L.; Kraffert, F.; Wang, R.; Zhang, C.; Bittl, R.; Behrends, J. Tuning Spin Dynamics in Crystalline Tetracene. *J. Phys. Chem. Lett.* **2019**, *10*, 1908−1913.

(45)   Wan, Y.; Wiederrecht, G. P.; Schaller, R. D.; Johnson, J. C.; Huang, L. Transport of Spin-Entangled Triplet Excitons Generated by Singlet Fission. *J. Phys. Chem. Lett.* **2018**, *9*, 6731−6738.

(46)   Burgdorff, G.; Kircher, T.; Lohmannsroben, H.-G. Photophysical Properties of Tetracene Derivatives in Solution. *Spectrochim. Acta A* **1988**, *44*, 1137–1141.

(47)   Katoh, R.; Suzuki, K.; Furube, A.; Kotani, M.; Tokumaru, K. Fluorescence Quantum Yield of Aromatic Hydrocarbon Crystals. *J. Phys. Chem. C* **2009**, *113*, 2961–2965.

(48)   Kanamaru, N. Radiationless Transition between Randomly Fluctuating Levels. S1-T2-T1 Intersystem Crossing in Condensed Phase. *Bull. Chem. Soc. Japan* **1982**, *55*, 3093–3096.

(49)   Kwiat, P. G.; Mattle, K.; Weinfurter, H.; Zeilinger, A.; Sergienko, A. V.; Shih, Y. New High-Intensity Source of Polarization-Entangled Photon Pairs. *Phys. Rev. Lett.* **1995**, *75*, 4337–4341.

(50)   Bardeen, C. J. Time Dependent Correlations of Entangled States with Nondegenerate Branches and Possible Experimental Realization Using Singlet Fission. *J. Chem. Phys.* **2019**, *151*, 124503.

(51)   Spano, F. C. The Spectral Signatures of Frenkel Polarons in H- and J-Aggregates. *Acc. Chem. Res.* **2010**, *43*, 429–439.

(52)   Yarmus, L.; Rosenthal, J.; Chopps, M. EPR of Triplet Excitons in Tetracene Crystals: Spin Polarization and the Role of Exciton Fission. *Chem. Phys. Lett.* **1972**, *16*, 477–481.

(53) Yong, C. K.; Musser, A. J.; Bayliss, S. L.; Lukman, S.; Tamura, H.; Bubnova, O.; Hallani, R. K.; Meneau, A.; Resel, R.; Maruyama, M.; Hotta, S.; Herz, L. M.; Beljonne, D.; Anthony, J. E.; Clark, J.; Sirringhaus, H. The Entangled Triplet Pair State in Acene and Heteroacene Materials. *Nat. Commun.* **2017**, *8*, 15953.

(54) Chen, M.; Nelson, M. D. K. J. N.; Bae, Y. J.; Harvey, S. M.; Schaller, R. D.; Young, R. M.; Wasielewski, M. R. Quintet-Triplet Mixing Determines the Fate of the Multiexciton State Produced by Singlet Fission in a Terrylenediimide Dimer at Room Temperature. *Proc. Nat. Acad. Sci.* **2019**, *116*, 8178–8183.

(55) Sanders, M. J. Y. T. S. N.; Kumarasamy, E.; Campos, L. M.; Sfeir, M. Y.; McCamey, D. R. Quintet Multiexciton Dynamics in Singlet Fission. *Nat. Phys.* **2016**, *13*, 182–188.

(56) R.Weiss, L.; Bayliss, S. L.; Kraffert, F.; Thorley, K. J.; Anthony, J. E.; Bittl, R.; Friend, R. H.; Rao, A.; Greenham, N. C.; Behrends, J. Strongly Exchange-Coupled Triplet Pairs in an Organic Semiconductor. *Nat. Phys.* **2016**, *13*, 176–181.

(57) Basel, B. S.; Zirzlmeier, J.; Hetzer, C.; Phelan, B. T.; Krzyaniak, M. D.; Reddy, S. R.; Coto, P. B.; Horwitz, N. E.; Young, R. M.; White, F. J.; Hampel, F.; Clark, T.; Thoss, M.; Tykwinski, R. R.; Wasielewski, M. R.; Guldi, D. M. Unified Model for Singlet Fission within a Non-Conjugated Covalent Pentacene Dimer. *Nat. Commun.* **2017**, *8*, 15171.

(58) Lubert-Perquel, D.; Salvadori, E.; Dyson, M.; Stavrinou, P. N.; Montis, R.; Nagashima, H.; Kobori, Y.; Heutz, S.; Kay, C. W. M. Identifying Triplet Pathways in Dilute Pentacene Films. *Nat. Commun.* **2018**, *9*, 4222.

(59) Matsuda, S.; Oyama, S.; Kobori, Y. Electron Spin Polarization Generated by Transport of Singlet and Quintet Multiexcitons to Spincorrelated Triplet Pairs during Singlet Fissions. *Chem. Sci.* **2020**, *11*, 2934–2942.

(60) Kobayashi, T.; Hirota, N. Bimolecular Quenching of Triplet Exciton in Crystalline P-Dibromobenzene. *Bull. Chem. Soc. Japan* **1977**, *50*, 1743–1745.

(61) Williams, D. F.; Adolph, J. Diffusion Length of Triplet Excitons in Anthracene Crystals. *J. Chem. Phys.* **1967**, *46*, 4252–4254.

(62) Lim, S.-H.; Bjorklund, T. G.; Spano, F. C.; Bardeen, C. J. Exciton Delocalization and Superradiance in Tetracene Thin Films and Nanoaggregates. *Phys. Rev. Lett.* **2004**, *92*, 107402.

(63) Camposeo, A.; Polo, M.; Tavazzi, S.; Silvestri, L.; Spearman, P.; Cingolani, R.; Pisignano, D. Polarized Superradiance from Delocalized Exciton Transitions in Tetracene Single Crystals. *Phys. Rev. B* **2010**, *81*, 033306.

(64) Voigt, M.; Langner, A.; Schouwink, P.; Lupton, J. M.; Mahrt, R. F.; Sokolowski, M. Picosecond Time Resolved Photoluminescence Spectroscopy of a Tetracene Film on Highly Oriented Pyrolytic Graphite: Dynamical Relaxation, Trap Emission, and Superradiance. *J. Chem. Phys.* **2007**, *127*, 114705.

(65) Kazzaz, A. A.; Zahlan, A. B. Temperature Dependence of Crystalline Tetracene Fluorescence. *J. Chem. Phys.* **1968**, *48*, 1242–1245.

(66) Venuti, E.; Valle, R. G. Della; Farina, L.; Brillante, A.; Masino, M.; Girlando, A. Phonons and Structures of Tetracene Polymorphs at Low Temperature and High Pressure. *Phys. Rev. B* **2004**, *70*, 104106/1-104106/8.

(67) Jankowiak, R.; Kalinowski, J.; Konys, M.; Buchert, J. Solid-State Transitions in Crystalline Tetracene. *Chem. Phys. Lett.* **1979**, *65*, 549–553.

(68) Sondermann, U.; Kutoglu, A.; Bassler, H. X-Ray Diffraction Study of the Phase Transition in Crystalline Tetracene. *J. Phys. Chem.* **1985**, *89*, 1735–1741.

(69) Sloan, G. J.; Mcghie, A. R. Purification of Tetracene: Vapor Zone Refining and Eutectic Zone Melting. *Mol. Cryst. Liq. Cryst.* **1972**, *19*, 17–37.

(70) Bridge, N. J.; Vincent, D. Fluorescence and Raman Spectra of Pure and Doped Anthracene Crystals at 4 K. *J. Chem. Soc. Farad. Trans. 2* **1972**, *68*, 1522–1535.

(71) Lyons, L. E.; Warren, L. J. Anthracene Fluorescence at Low Temperatures. I. Purified Single Crystals. *Aust. J. Chem.* **1972**, *25*, 1411–1425.

(72) Kondratenko, P. A.; Khutornaya, L. A.; Shpak, M. T. Effect of Lattice Defects on the Luminescence Spectra of Anthracene Crystals. *Zhu. Prik. Spekt.* **1980**, *33*, 856–859.

(73) Rice, S. A.; Morris, G. C.; Greer, W. L. Conjecture Concerning the Width of the Lowest Singlet-Singlet Transition in Crystalline Anthracene. *J. Chem. Phys.* **1970**, *52*, 4279–4287.

(74) Zhang, B.; Zhang, C.; Xu, Y.; Wang, R.; He, B.; Liu, Y.; Zhang, S.; Wang, X.; Xiao, M. Polarization-Dependent Exciton Dynamics in Tetracene Single Crystals. *J. Chem. Phys.* **2014**, *141*, 244303.

(75) Frolov, S. V.; Kloc, C.; Schon, J. H.; Batlogg, B. Transient Spectroscopy of Tetracene Single Crystals. *Chem. Phys. Lett.* **2001**, *334*, 65–68.

(76) Wan, Y.; Guo, Z.; Zhu, T.; Yan, S.; Johnson, J.; Huang, L. Cooperative Singlet and Triplet Exciton Transport in Tetracene Crystals Visualized by Ultrafast Microscopy. *Nat. Chem.* **2015**, *785–792*.

(77) Thorsmolle, V. K.; Averitt, R. D.; Demsar, J.; Smith, D. L.; Tretiak, S.; Martin, R. L.; Chi, X.; Crone, B. K.; Ramirez, A. P.; Taylor, A. J. Morphology Effectively Controls Singlet-Triplet Exciton Relaxation and Charge Transport in Organic Semiconductors. *Phys. Rev. Lett.* **2009**, *102*, 017401.

(78) Birech, Z.; Schwoerer, M.; Schmeiler, T.; Pflaum, J.; Schwoerer, H. Ultrafast Dynamics of Excitons in Tetracene Single Crystals. *J. Chem. Phys.* **2014**, *140*, 114501.

(79) Arias, D. H.; Ryerson, J. L.; Cook, J. D.; Damrauer, N. H.; Johnson, J. C. Polymorphism Influences Singlet Fission Rates in Tetracene Thin Films. *Chem. Sci.* **2016**, *7*, 1185–1191.

(80) Grumstrup, E. M.; Johnson, J. C.; Damrauer, N. H. Enhanced Triplet Formation in Polycrystalline Tetracene Films by Femtosecond Optical Pulse Shaping. *Phys. Rev. Lett.* **2010**, *105*, 257403.

(81) Campillo, A. J.; Hyer, R. C.; Shapiro, S. L.; Swenberg, C. E. Exciton Interactions in Crystalline Tetracene Studied by Single Picosecond Pulse Excitation. *Chem. Phys. Lett.* **1977**, *48*, 495–500.

(82) Campillo, A. J.; Shapiro, S. L.; Swenberg, C. E. Picosecond Measurements of Exciton Migration in Tetracene Crystals Doped with Pentacene. *Chem. Phys. Lett.* **1977**, *52*, 11–15.

(83) Vaubel, G.; Baessler, H. Diffusion of Singlet Excitons in Tetracene Crystals. *Mol. Cryst. Liq. Cryst.* **1970**, *12*, 47–56.

(84) Smith, A. W.; Weiss, C. Fluorescence Decay Time Measurements in Tetracene Crystals. *Chem. Phys. Lett.* **1972**, *14*, 507–511.

(85) Klein, G. Kinematics of Triplet Pairs in Anthracene and Tetracene Crystals. *Chem. Phys. Lett.* **1978**, *57*, 202–206.

(86) Fleming, G. R.; Millar, D. P.; Morris, G. C.; Morris, J. M.; Robinson, G. W. Exciton Fission and Annihilation in Crystalline Tetracene. *Aust. J. Chem.* **1977**, *30*, 2353–2359.

(87) Alfano, R. R.; Shapiro, S. L.; Pope, M. Fission Rate of Singlet Excitons in a Tetracene Single Crystal Measured with Picosecond Laser Pulses. *Opt. Comm.* **1973**, *9*, 388–391.

(88)   Lopez-Delgado, R.; Miehe, J. A.; Sipp, B. Fluorescence Decay Time Measurements in Tetracene Crystals Excited with Synchrotron Radiation. *Opt. Comm.* **1976**, *19*, 79–82.

(89)   Burdett, J. J.; Müller, A. M.; Gosztola, D.; Bardeen, C. J. Excited State Dynamics in Solid and Monomeric Tetracene: The Roles of Superradiance and Exciton Fission. *J. Chem. Phys.* **2010**, *133*, 144506.
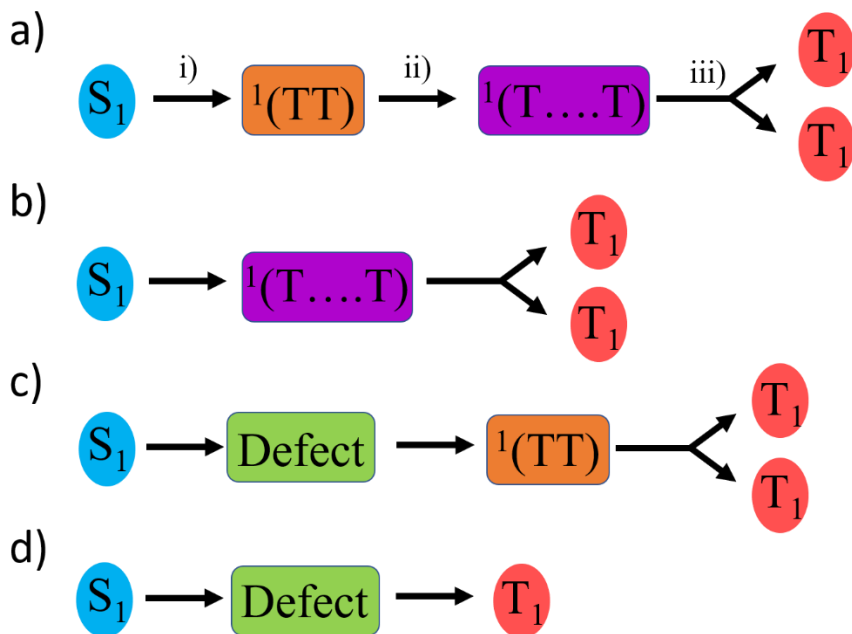
Fig. 1. Mechanisms for singlet relaxation in crystalline TET that can create triplet excitons: a) Sequential pathway for singlet fission, with 3 steps: i) initial creation of bound triplet pair from singlet S_1, ii) triplet pair separation, iii) spin decoherence into uncorrelated, independent triplet excitons. b) Direct creation of spatially separated triplet pair. c) Singlet trapping at a defect followed by singlet fission. d) Singlet trapping at a defect followed by intersystem crossing.
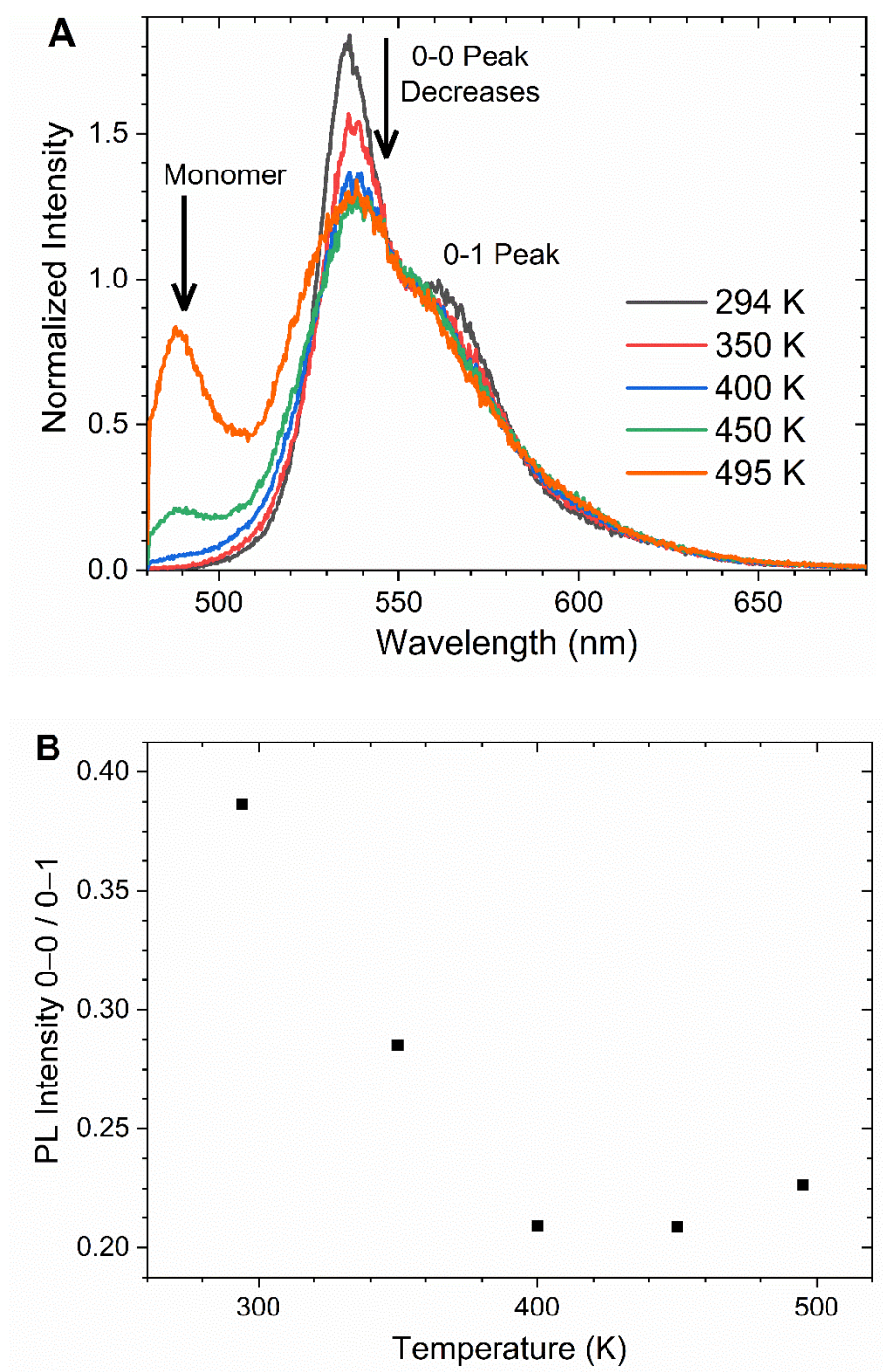
Fig. 2. A) Temperature dependent fluorescence spectra of a tetracene single crystal submerged in fomblin oil. At elevated temperatures, the intensity of the 0-0 peak (535 nm) decreases. Above 450 K, monomeric fluorescence emerges (490 nm) as the crystal partially dissolves in the protective oil. B) The ratio of the 0-0 peak intensity to the 0-1 peak intensity is plotted as a function of temperature. The intensity is determined from Gaussian fits to the spectra at each temperature.
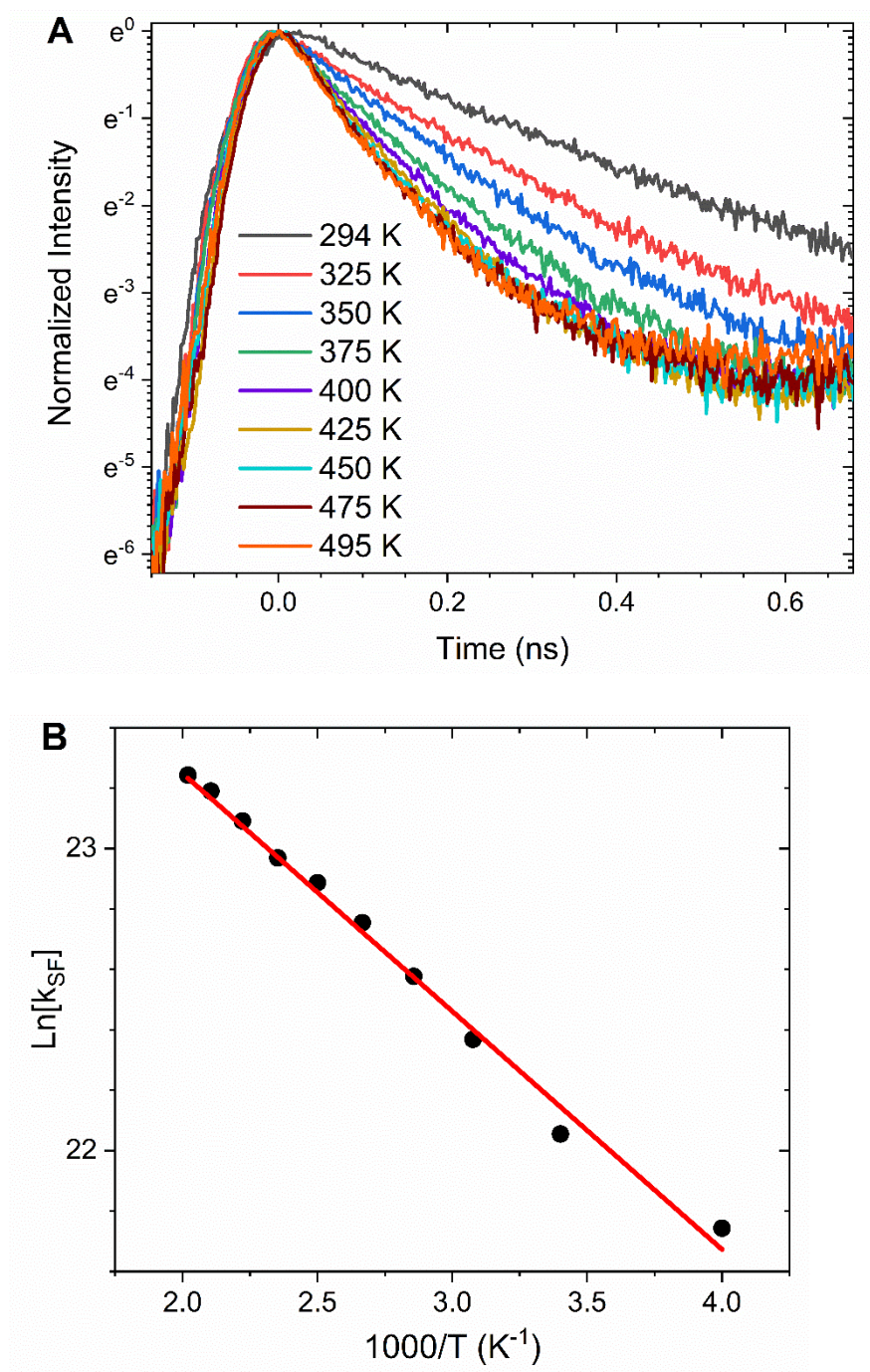
Fig. 3. A) The temperature-dependent, early-time fluorescence decay of single crystal tetracene submerged in fomblin oil showing a more rapid decay of the singlet at elevated temperatures. B) An Arrhenius plot of the singlet decay rate (k_{S1}) as a function of temperature. k_{S1} is determined from fitting the decays in Fig 3A with exponential functions. A linear fit (red line) yields an activation energy of 550 cm^{-1}.
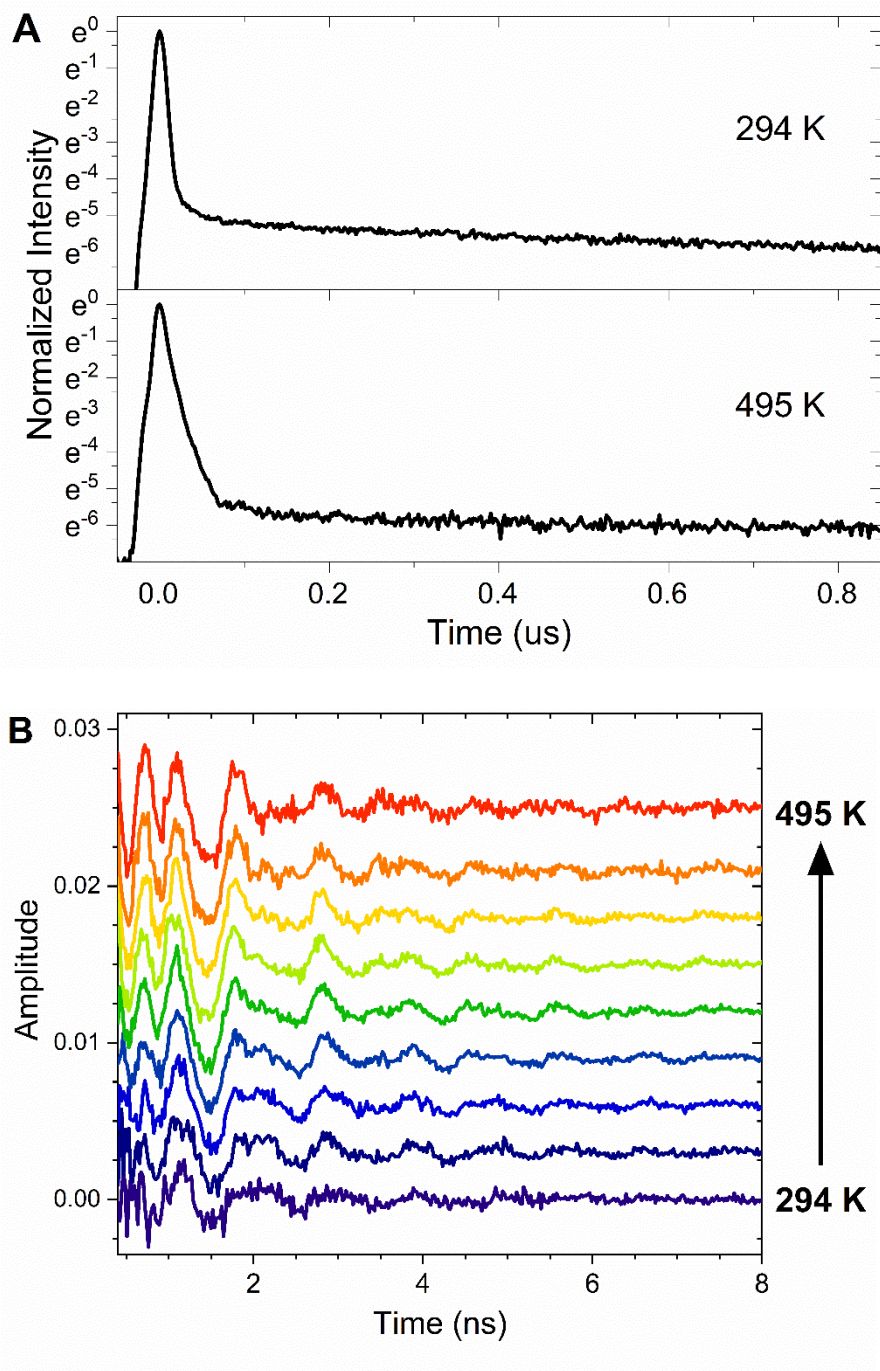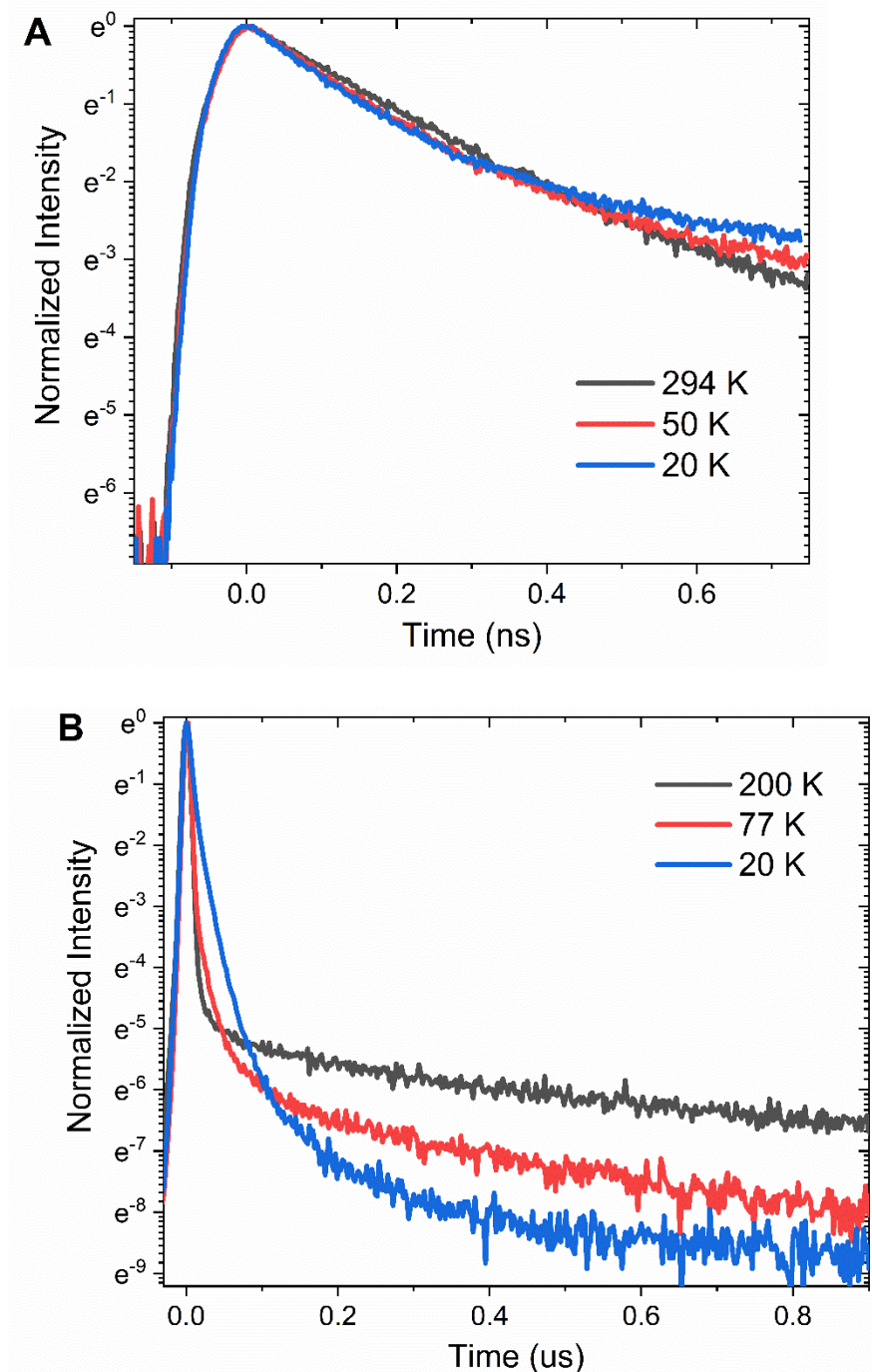
Fig. 4. A) The fluorescence decay of single crystal tetracene submerged in fomblin oil in a 1 µs window at 294 K (top) and 495 K (bottom). An initial rapid decay of the singlet over ≈100 ns turns into a long-lived delayed fluorescence at both temperatures. At 495 K, the initial decay (t < 100 ns) appears slower due to residual PL from monomeric tetracene; however, the monomer does not contribute to the signal for t > 100 ns. B) The quantum beats extracted from the fluorescence decays of single crystal tetracene submerged in fomblin oil as a function of temperature.
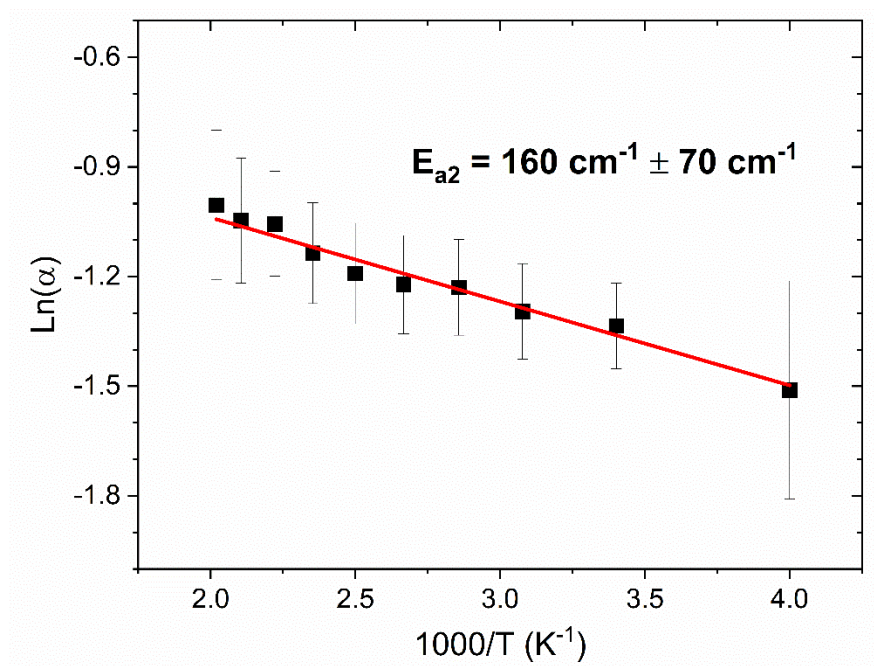
Fig. 5. An Arrhenius plot of the damping constant, α, extracted from the quantum beats using Equation (2). The error bars represent the relative error in α obtained from the fit of Equation (2) to the oscillations. The linear fit yields an activation energy of 160 cm^{-1} ± 70 cm^{-1}.
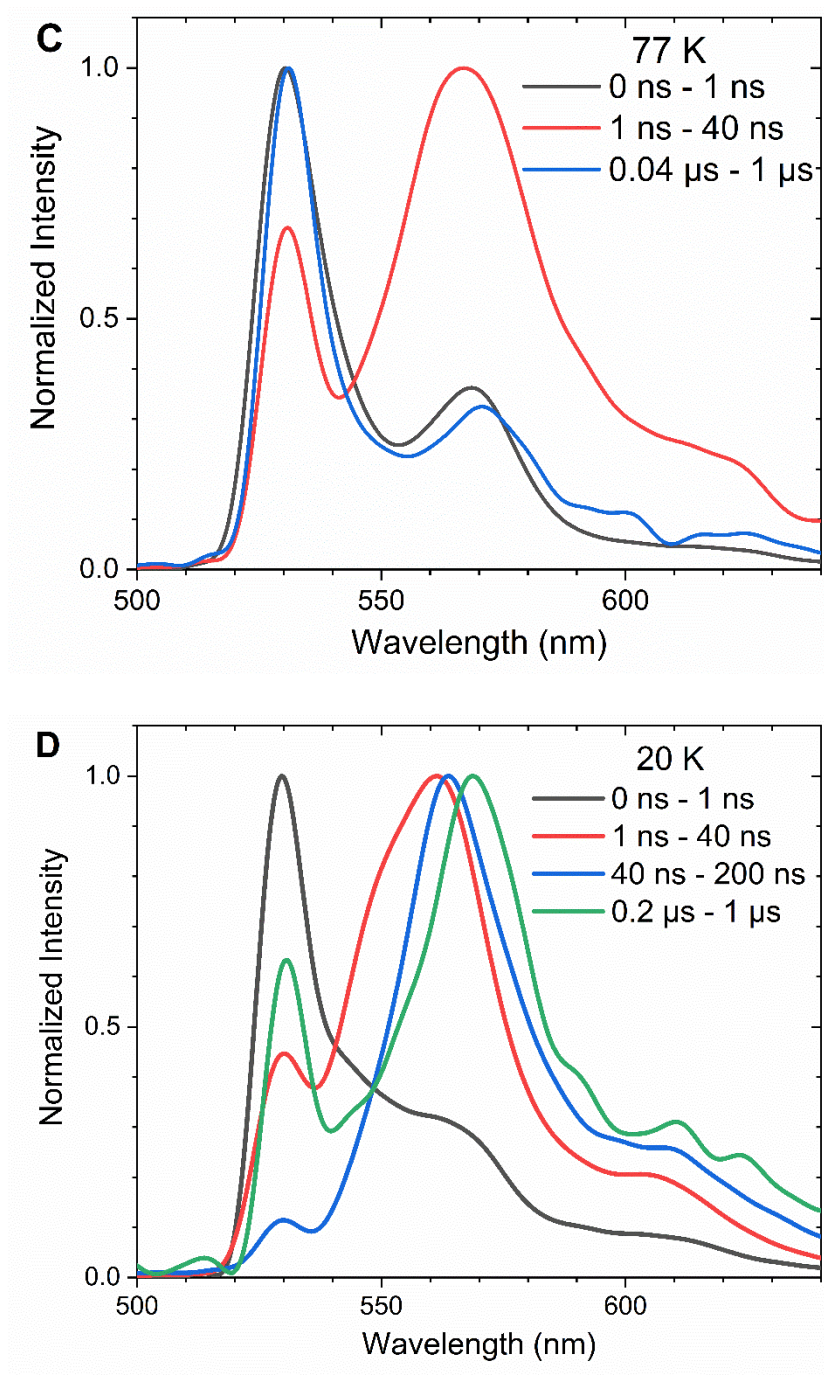
Fig. 6. A) The early-time fluorescence decay of a single tetracene crystal showing a rapid singlet decay even at cryogenic temperatures. B) The long-time fluorescence decay of a single tetracene crystal below room temperature. The long-lived delayed fluorescence observed for T > 200 K decays more rapidly as the temperature is lowered.
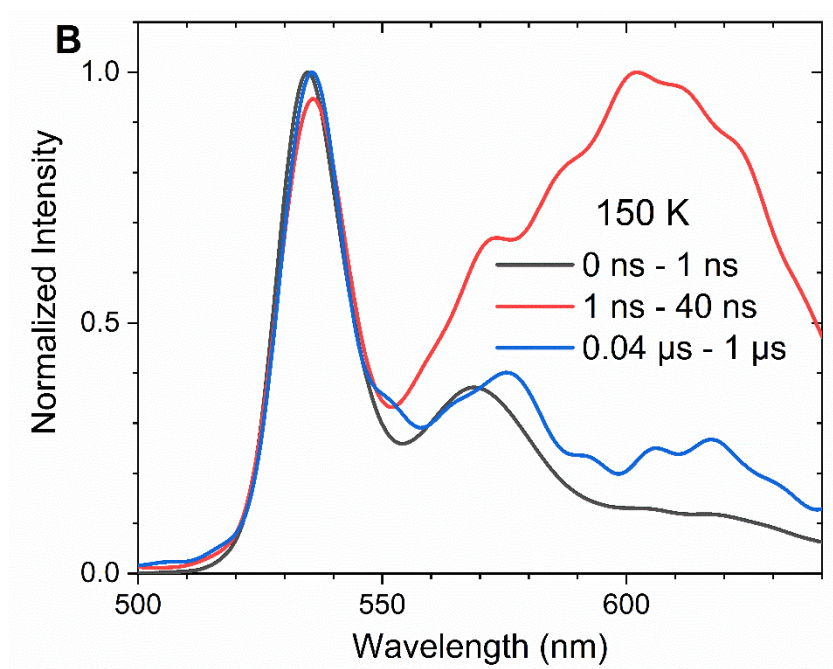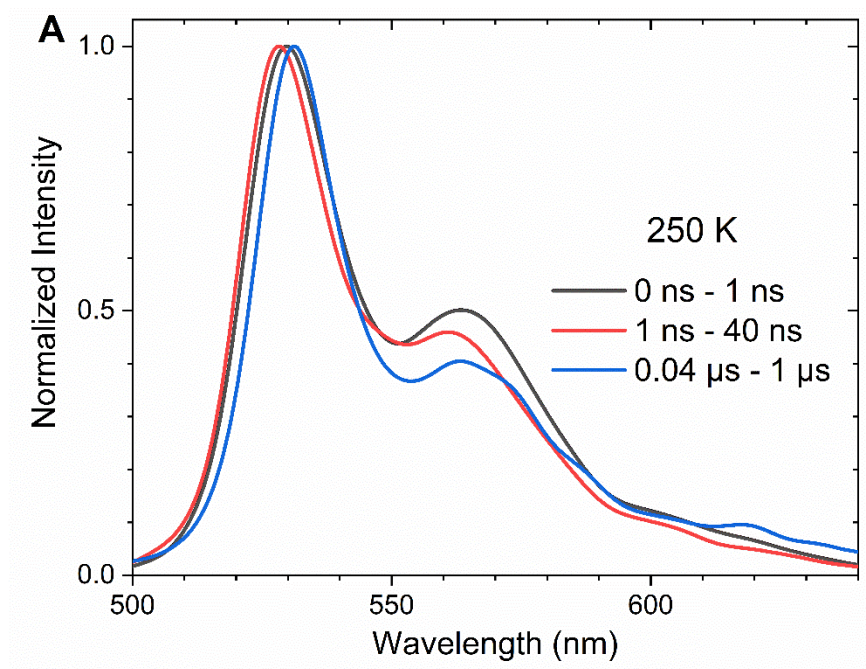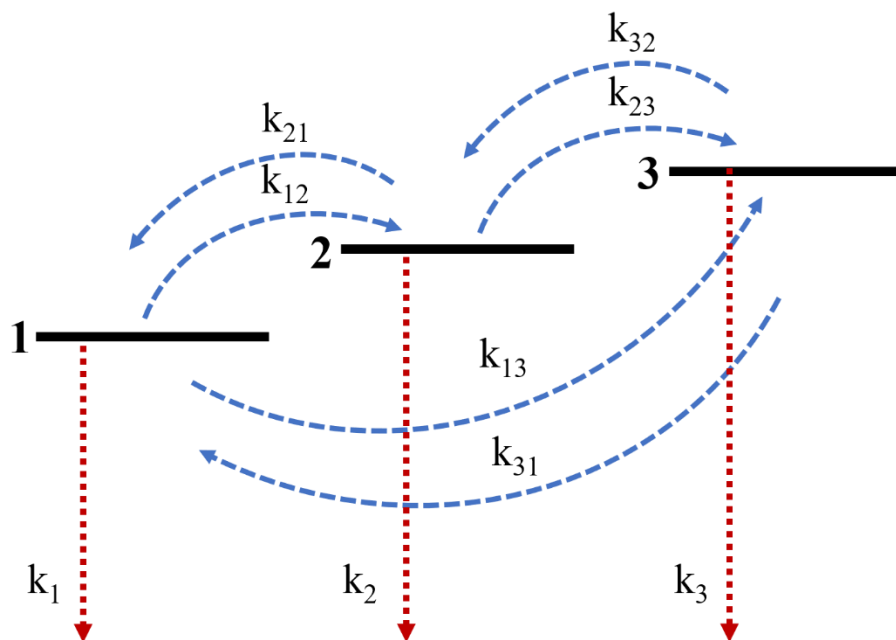
Fig. 7. The spectral evolution of a tetracene single crystal at (A) 250 K, (B) 150 K, (C) 77 K and (D) 20 K. At 150 K and 77 K, a redshifted feature briefly emerges before the original S_1 emission is recovered at later times. At 20 K, a redshifted feature also appears, but the original S_1 spectrum is never fully recovered at later times. Each spectral slice has been smoothed for clarity.

Fig. 8. 3 level diagram based on Equations (3a-c), where level 1 corresponds to S_1, level 2 corresponds to the emissive $^1(TT)$ state, and level 3 corresponds to the T_1 reservoir. Rate constants are defined in the text.